Tellus (1999), 51A, 574–587
Printed in UK. All rights reserved



TELLUS
ISSN 0280–6495

# Upstream development in idealized baroclinic wave experiments

By HEINI WERNLI[1]*, MELVYN A. SHAPIRO[2] and JÜRG SCHMIDLI[1], [1]*Institute for Atmospheric Science, ETH Hönggerberg, CH-8093 Zürich, Switzerland;* [2]*NOAA/Environmental Technology Laboratory, Boulder CO, USA*

(Manuscript received 7 October 1998; in final form 21 June 1999)

ABSTRACT

An idealized dry primitive equation model on the $f$-plane is used to study upstream (and downstream) baroclinic wave development. The simulations are initiated with localized finite amplitude and vertically evanescent perturbations, specified either as upper-level potential vorticity or surface potential temperature anomalies. The nonlinear evolution of these nonmodal perturbations leads to the generation of large-scale upper-level induced primary and downstream surface cyclones, and of distinctively smaller, shallow and more slowly intensifying upstream systems. It is shown that in particular the genesis and evolution of upstream cyclones is highly sensitive to the scale of the initial perturbation. Narrow upper-level troughs (or zonally confined surface temperature anomalies) are favorable for upstream development, whereas no or only weak upstream activity occurs with broad planetary-scale troughs (or zonally extended surface temperature anomalies) as initial perturbations. It is proposed that this sensitivity property of upstream development is qualitatively related to the dispersion characteristics of surface edge waves.

The shortcomings of the present approach are discussed, and some consideration is given to the occurrence of upstream cyclogenesis in the real atmosphere, to the relationship with earlier concepts of secondary cyclogenesis, and to possible implications for the issue of predictability of extratropical weather systems.

## 1. Introduction

Hitherto, the major part of idealized channel model experiments for baroclinic wave development focussed on the evolution, structure and energetics of primary cyclones which grow from a specified initial perturbation on two-dimensional jet-like basic states (see for instance the reviews by Davies (1994) and Simmons (1994)). The traditional approach is to initialize the numerical integrations with the most unstable normal-mode, and this leads to a baroclinic wave train with a prescribed zonal periodicity (Hoskins and West, 1979; Davies et al., 1991). Another approach is to use (finite amplitude) localized initial perturbations. This introduces additional degrees of freedom for the setup of the simulations, e.g., the structure and amplitude of the nonmodal perturbation and of the zonal dimension of the integration domain. The present work falls into this second category, and in the following a brief summary is given of results from pertinent earlier investigations.

In a pioneering study, Simmons and Hoskins (1979) have shown that a localized barotropic initial perturbation within a long channel can lead not only to the development of a primary cyclone but also to the generation of secondary systems up- and downstream of the traveling primary cyclone later in the development. They noted that up- and downstream systems are distinctively

* Corresponding author.

different, in that upstream (downstream) developments first appear at the surface (at the tropopause level) followed by an upward (downward) development. These "bottom-up" versus "top-down" growth characteristics can be regarded as idealized analogs of the Petterssen and Smebye (1971) type A and B categories for cyclone life cycles. The experiments by Simmons and Hoskins further revealed that upstream cyclones are typically of smaller scale than primary and downstream systems, and that they first appear close to the position of the initial perturbation. The dynamical understanding for the characteristics of upstream development constitutes one of the main goals of the present study.

Orlanski and Chang (1993) studied the up- and downstream energy dispersion within linear and nonlinear baroclinic wave experiments. From a detailed analysis of the ageostrophic geopotential fluxes they inferred that these fluxes contribute significantly to up- and downstream developments. Both these studies used barotropic initial perturbations and did not consider for instance the smaller-scale frontal structures which evolve during the nonlinear evolution of the baroclinic waves. Simulations with a higher-resolution primitive equation model and a vertically decaying finite amplitude upper-level initial perturbation (Shapiro et al., 1998) confirmed the different scale and vertical structure of up- and downstream developing systems. In addition the different evolutions of the surface frontal palette associated with up- and downstream cyclones was illustrated, and it was shown that in particular the upstream structures are susceptible to the ambient flow.

The phenomenon of upstream cyclogenesis within idealized dry numerical simulations using localized initial perturbations is examined further in this study. The focus is on the dynamical understanding of the influence of the scale of the initial perturbation on the genesis and evolution of upstream cyclones. After a brief description of the model setup (Section 2), the results from a first experiment of upper-level induced cyclogenesis are presented and analyzed in Section 3. Upstream development is then interpreted with the aid of the dispersion relationship for surface edge waves (Davies and Bishop, 1994), and a series of numerical simulations with differing initial perturbations is examined in Section 4 in order to validate the inferences from the linear analysis.

## 2. The model and set-up of the numerical simulations

The primitive equation model used for the purpose of this study is the same as in the idealized studies by Wernli et al. (1998) and Shapiro et al. (1998), that is an $f$-plane version of the operational limited-area weather forecast model of the German Weather Service (Europa-Model, Majewski, 1991). It is hydrostatic, and except for a second order horizontal diffusion all other physical parametrization schemes were inoperative.

In the present study simulations have been performed with a horizontal grid spacing of $\sim 75$ km and 26 constant pressure levels that range from about 1000 to 100 hPa (with a rigid lid upper boundary condition). Periodic boundary conditions have been applied in the zonal direction, and meridionally the lateral boundary conditions are accommodated with the relaxation technique of Davies (1976). The integration domain covers about $16\,800 \times 7000$ km ($217 \times 91$ grid points).

The initial conditions comprise a two-dimensional baroclinic jet-like basic state and a finite amplitude initial perturbation. The baroclinic jet basic state is portrayed in Fig. 1. It has a width of $\sim 2000$ km and the jet speed maximum corresponds to $44\ \mathrm{m\,s^{-1}}$. (The same jet structure but

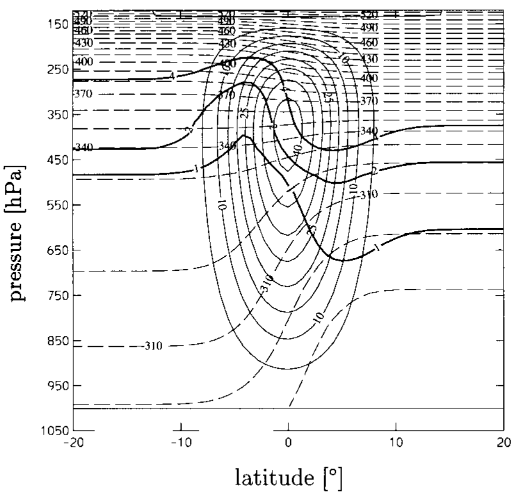


*Fig. 1.* South–north oriented vertical section across the baroclinic jet basic state. Solid lines mark the zonal wind speed (contour interval $5\ \mathrm{m\,s^{-1}}$), dashed lines potential temperature (contour interval 10 K), and the bold lines correspond to the 1, 2 and 4 pvu isolines.

Table 1. *Parameters for the specification of the initial perturbations for the experiments discussed in this study*

| Name | $A_l$ (pvu) | $A_c$ (pvu) | $L_x$ (km) | $L_y$ (km) | $d$ (km) | $a$ (K) | $l_x$ (km) | $l_y$ (km) |
|---|---|---|---|---|---|---|---|---|
| UL1 | 0 | 2 | 600 | 600 | — | 0 | — | — |
| UL2 | 0 | 2 | 900 | 600 | — | 0 | — | — |
| UL3 | −2 | 2 | 450 | 600 | 1500 | 0 | — | — |
| S1W | 0 | 0 | — | — | — | 2.1 | 1600 | 800 |
| S2W | 0 | 0 | — | — | — | 8.4 | 400 | 800 |
| S2C | 0 | 0 | — | — | — | −8.4 | 400 | 800 |

For an explanation of the parameters see eqs. (1), (2).

with a larger amplitude has been used for the single-jet simulations by Shapiro et al. (1998).)

Experiments with different initial perturbations are carried out in this study, specified either in terms of quasi-geostrophic potential vorticity (PV) near the tropopause level ("upper-level induced cyclogenesis", Sections 3 and 4.3) or potential temperature at the surface ("surface induced cyclogenesis", Subsection 4.2). In both cases the perturbation consists of either a single elliptic or circular anomaly or a zonally aligned pair of anomalies. They are specified in Cartesian space $(x, y, z)$ and a quasi-geostrophic PV inversion tool (Fehlmann, 1997) is used to derive balanced initial conditions for the numerical integrations. The PV anomalies used in this study take the form:

$$q'(x, y, z) = \left\{ A_c \exp\left[ -\left(\frac{x}{L_x}\right)^2 \right] + A_l \exp\left[ -\left(\frac{x+d}{L_x}\right)^2 \right] \right\} \times \left\{ \exp\left[ -\left(\frac{y}{L_y}\right)^2 \right] \times \exp\left[ -\left(\frac{z-z_0}{L_z}\right)^2 \right] \right\}. \quad (1)$$

$A_c$ and $A_l$ denote the amplitude of the central and left anomaly, respectively, where the central anomaly is located at $(0, 0, z_0)$ and the left anomaly is shifted by a distance $d$ in the zonal direction. In the case of surface potential temperature perturbations the form of the anomaly located at $(0, 0, 0)$ with amplitude $a$ is given by:

$$\theta'(x, y) = a \left\{ 1 + \left(\frac{x}{l_x}\right)^2 + \left(\frac{y}{l_y}\right)^2 \right\}^{-3/2}. \quad (2)$$

Table 1 gives an overview of the parameters selected for the experiments which will be discussed in this study ($z_0$, the height of the PV anomalies is always 8 km; and the vertical decay length $L_z$ equals 10 km).

## 3. Up- and downstream development: an example

In this section, results from a first simulation (UL1) of upper-level induced baroclinic wave development are presented. The initial perturbation consists of a positive circular finite-amplitude PV anomaly located near the level of the tropopause (cf. Table 1). During the time period of 1 week, a primary (P), two downstream (D1, D2) and one upstream cyclone (U) develop at the surface (Fig. 2) in parallel with three anticyclones and several distinct frontal structures. The primary cyclone P grows slightly to the east of the initial upper-level perturbation and develops a T-bone surface frontal configuration by day 4–5 with a pronounced warm-air seclusion (Figs. 2e, g). At day 6, the surface vortex is vertically aligned with the wrapped-up stratospheric PV anomaly (Fig. 2j) and at the surface the cold front overtakes the warm front resulting in a completely occluded system one day later (Fig. 2k).

At day 4, there is a first indication of a downstream cyclone (D1) in the surface pressure field (Fig. 2e), but already one day earlier a wave-like disturbance can be recognized in the upper-level PV field about 3000 km to the east of the primary cyclone (Fig. 2d). This upper-level anomaly amplifies rapidly into a pronounced PV streamer (Figs. 2j, l) concomitantly with an intense surface development. In the early stage the frontal evolu-

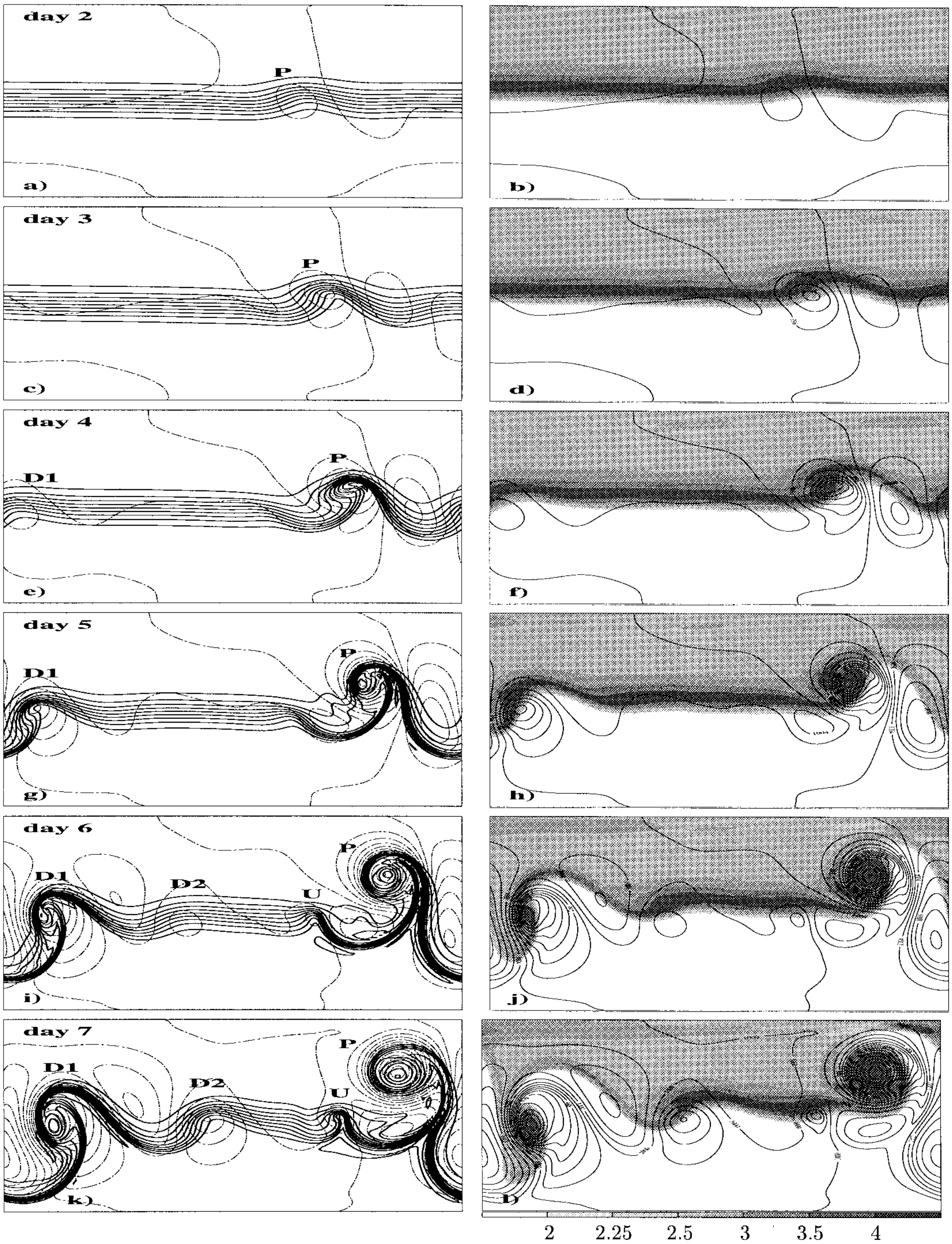


*Fig. 2.* Flow evolution for the numerical simulation UL1. In the left panels solid lines indicate the surface potential temperature field (contour interval 2 K) and dash-dotted lines the surface pressure distribution (contour interval 4 hPa). The right panels show the PV field on the 330 K isentropic surface (shaded, see scale below lowest right panel) and again surface pressure (solid lines). The diagrams cover a domain of 15 870 × 6660 km.

tion associated with D1 is comparable to the primary cyclone, but in the mature stage, D1 remains unoccluded with a marked frontal fracture and a relatively wide open warm sector (Figs. 2i, k).

A very similar development (D2) starts after day 5 about 4000 km downstream of D1 (Figs. 2h, j). Note that for both downstream cyclones the freely evolving upper-level PV anomaly has an asymmetric structure (with a stronger PV gradient near the western flank and a tilted structure in the vertical (not shown)), unlike the predefined initial perturbation. Possibly this leads to the strikingly different upper-level evolution for the primary versus the downstream cyclones, which is also reflected at the surface by the differing frontal evolution and meridional displacement of the depressions.

Finally the upstream cyclone U shows up at day 6 in the surface pressure field (Fig. 2i). Genesis of this cyclone takes place about 2500 km upstream of the actual position of the center of the primary system P, at the trailing end of its bent cold front. It is important to note that, at that time, at the position of cyclogenesis no disturbance can be seen at upper-levels (Fig. 2j). During the next day the upstream depression intensifies moderately and a surface frontal structure is established with a pronounced warm and a weaker and short cold front (Fig. 2k). The upper-level PV field shows a weak undulation to the west of U (Fig. 2l), due to the proximity of D2 it is not clear whether this is a downstream effect of D2 or induced by the surface thermal pattern, and the surface diagrams (Figs. 2i, k) clearly reveal that U has a distinctively smaller scale than the primary and downstream cyclones (a diameter of less than 1000 km compared to about 2000 km for the simultaneously growing D2).

Fig. 3 gives an alternative view of the development which resembles the classical visualization of up- and downstream development by Simmons and Hoskins (1979). Displayed is the vorticity perturbation (i.e., the deviation from the zonal mean) meridionally averaged over the central 5000 km of the channel. It shows the initial disturbance at upper-levels (Fig. 3a) and the subsequent downstream generation of a train of negative and positive upper-level perturbations (the first negative vorticity anomaly occurs at day 1 (not shown), the second positive (negative) one at day 2.5 (3.5) and the 3rd positive perturbation at day 5), with a typical wavelength of almost 4000 km. These primary and downstream perturbations intensify and extend vertically down to the surface with a westward tilt which is characteristic for baroclinic growth. In contrast to this the vorticity perturbation associated with the upstream development is horizontally more confined and has clearly a vertically evanescent structure (Figs. 3d–f). This analysis of the evolution allows to observe genesis of the upstream cyclone U already at day 5, only about 2000 km to the east of the position of the initially imposed perturbation (Fig. 3d). At the same location a second event of upstream cyclogenesis is weakly indicated at day 7 (Fig. 3f). Note that the zonal separation of the two upstream features is roughly half of that of the primary and downstream depressions.

A final analysis of this simulation is presented in Fig. 4 which illustrates the phenomenon of up- and downstream development from the PV perspective. Within this framework, cyclogenesis can be regarded as the generation, self-development and interaction of interior PV and surface potential temperature anomalies. The term "anomaly" refers to the deviation from a suitable climatological mean or in the present case of idealized simulations from the two-dimensional basic state. Positive (negative) PV and warm (cold) surface potential temperature anomalies are associated with vertically decaying cyclonic (anticyclonic) circulations and the vertical penetration is generally weak for anomalies with a small horizontal scale and under strongly stratified conditions (see for instance Bishop and Thorpe (1994)). Fig. 4 shows the evolving train of upper-level PV and surface potential temperature anomalies at three different time instances of the numerical simulation. By day 4 the initial upper-level disturbance (label I) has developed into an S-shaped feature. The advection associated with its cyclonic wind field led to the downstream generation of a warm surface temperature anomaly (cf. Hoskins et al., 1985) and a negative upper-level PV disturbance (cf. the concept for horizontal up/downstream development illustrated by Thorncroft and Hoskins (1990, their Fig. 20)). Note that this process is intrinsically nonlinear in that the simultaneous growth of the surface and upper-level anomalies is enhanced through their mutual interaction. In the downstream direction this mechan-

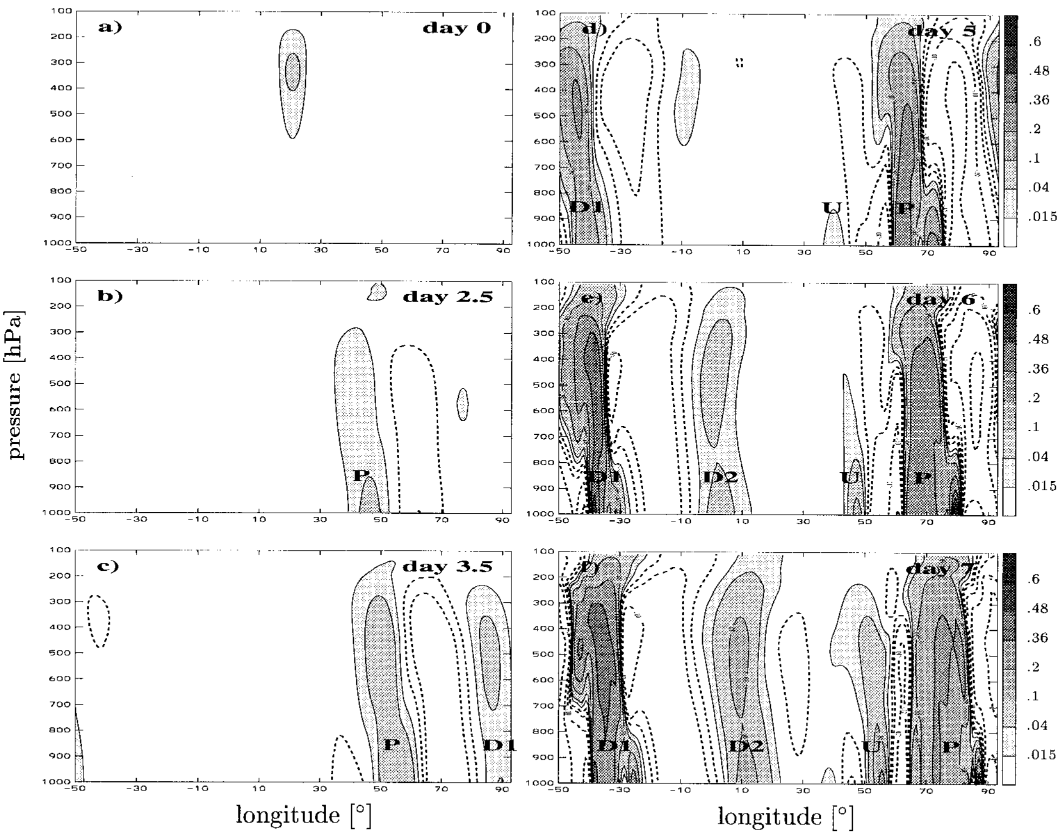


*Fig. 3.* West–east oriented vertical sections showing the meridionally averaged vorticity perturbation for the simulation UL1 (in units of *f*, see scale beside panels).

ism is very efficient as revealed by the generation (and rapid development) of the two downstream cyclones D1 and D2 within a time period of 6 days (the warm surface temperature anomalies associated with D1 and D2 are labeled in Fig. 4). However in the upstream direction the generation of new anomalies through advection is much slower. The cold surface temperature disturbance which has developed by day 4 (Fig. 4a) seems to be not strong enough to induce a substantial disturbance at upper-levels. And at the surface it is only at day 5.5 that a very tiny warm anomaly is generated through the anticyclonic flow associated with the cold anomaly (Fig. 4b) which constitutes the narrow warm sector of the upstream cyclone U one day later (Fig. 4c).

To summarize it was found that the dispersion of the upper-level disturbances is in the downstream direction and leads to the generation of PV anomalies which are large enough to induce and interact with surface temperature anomalies leading to synoptic-scale downstream depressions. On the other hand upstream development takes place predominantly at the surface through dispersion of surface temperature anomalies, is slower and associated with smaller scales. These results are in harmony with the study of Orlanski and Chang (1993) who found downstream (upstream) energy dispersion at the upper (lower) levels in their linear Eady experiment. However the issue of the small scales associated with the upstream development merits further consideration.

## 4. Sensitivity of upstream development on the scale of the initial perturbation

The simulation in Section 3 has revealed several important characteristics of upstream cyclones

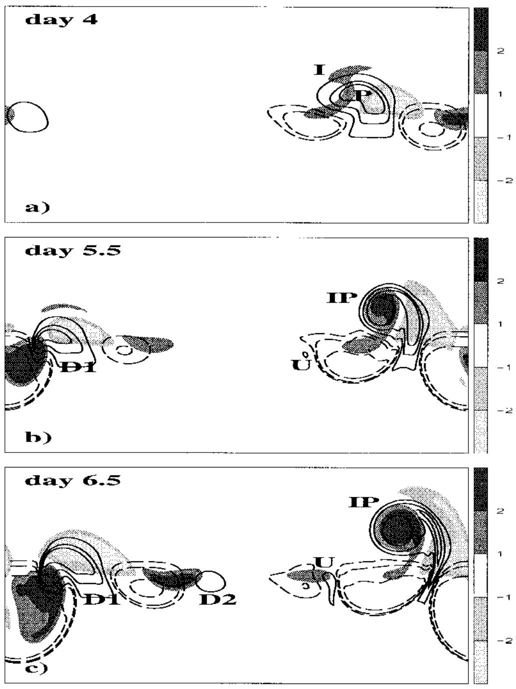


*Fig. 4.* Surface potential temperature and upper-level potential vorticity anomalies (deviations from the basic state) for the simulation UL1. Positive (negative) PV anomalies are indicated by dark (light) shading, and solid (dashed) lines denote warm (cold) surface temperature disturbances. The label I marks the initial positive upper-level PV anomaly.

which will be analyzed in more detail now. The fact that these systems first appear as a warm surface potential temperature anomaly (if considered within the PV framework) indicates that an analysis of the properties of such anomalies could be rewarding for the understanding of the generation and development of upstream cyclones. In the following the dispersion properties of surface edge waves (or neutral Rossby waves) in the classical Eady model system are re-examined (Subsection 4.1). It will be shown that qualitative inferences from this simple linear investigation help to formulate hypotheses for the sensitivity of upstream development to the initial conditions. In Subsections 4.2 and 4.3 a series of numerical experiments will be presented to verify these hypotheses.

### *4.1. Linear dispersion of surface edge waves*

Following the approach (and notation) of Davies and Bishop (1994), the semi-infinite Eady model system is considered, that is the quasi-geostrophic flow of an incompressible atmosphere on an $f$-plane above a rigid bounding surface at $z=0$. The basic state has a uniform background stratification ($N^2$) and uniform baroclinic shear, $\bar{U}=\Lambda z$. The lower boundary condition is given by the linearized, adiabatic form of the thermodynamic equation applied at $z=0$:

$$\left(\frac{\partial}{\partial t}+\bar{U}\frac{\partial}{\partial x}\right)\frac{\partial \psi'}{\partial z}-\Lambda\frac{\partial \psi'}{\partial x}=0, \tag{3}$$

with $\psi'$ denoting the perturbation geostrophic streamfunction. Consider a solution of this flow system taking the form of a vertically evanescent surface edge wave, i.e., a pure lower boundary wave with zero interior potential vorticity:

$$\psi' = A\sin(kx-\omega t)\cos(ly)\mathrm{e}^{-\mu z}, \tag{4}$$

where $\mu^2=(N^2/f^2)(k^2+l^2)$, and $(k, l)$ are the zonal and meridional wavenumbers, respectively. Insertion of eq. (4) into (3) yields the following dispersion relationship for surface edge waves:

$$\omega(k, l)=\bar{U}k+\frac{f}{N}\frac{\Lambda k}{\sqrt{k^2+l^2}}, \tag{5}$$

and the zonal group velocity is given by

$$u_\mathrm{g}=\frac{\partial\omega}{\partial k}=\bar{U}+\frac{f}{N}\frac{\Lambda l^2}{(k^2+l^2)^{3/2}}. \tag{6}$$

Equation (6) shows that the zonal group velocity relative to the mean flow is towards the east ($u_\mathrm{g}-\bar{U}>0$), and that surface edge waves are generally dispersive, with a slower (faster) energy propagation for waves with larger (smaller) zonal wavenumbers $k$ (for a fixed value of $l\neq 0$). (An exception is the one-dimensional case ($l=0$), where eq. (5) reduces to $\omega(k)=\bar{U}k+(f/N)\Lambda$ and the group velocity becomes equal to the surface mean flow, independent of the wavenumber, $u_\mathrm{g}=\bar{U}$. This situation has been analyzed for instance by Thorncroft and Hoskins (1990, Appendix).) Note also that for both the Eady model system and the basic state flow used for the numerical integrations (cf. Fig. 1) the surface background flow vanishes: $\bar{U}(z=0)=0$.

To estimate the typical magnitude of the zonal group velocity and the dispersion effect, eq. (6)

can be rewritten in the following form:

$$u_{\mathrm{g}} = \bar{U} + \underbrace{\frac{f}{N}\frac{\Lambda}{2^{3/2}l}}_{u_{\mathrm{g}}^*}\underbrace{\left[\frac{2}{1+(k/l)^2}\right]^{3/2}}_{\mathscr{F}}.$$

Here $u_{\mathrm{g}}^*$ corresponds to the group velocity relative to the mean flow for a symmetric disturbance ($k = l$), and $\mathscr{F}$ denotes a geometric form factor. Using appropriate values for the parameters* ($f = 10^{-4}\,\mathrm{s}^{-1}$, $N = 10^{-2}\,\mathrm{s}^{-1}$, $\Lambda = 4 \cdot 10^{-3}\,\mathrm{s}^{-1}$, and $l = 2\pi/4000\,\mathrm{km} \simeq 1.5 \cdot 10^{-6}\,\mathrm{m}^{-1}$) yields a value of $10\,\mathrm{ms}^{-1}$ (or $820\,\mathrm{km\,day}^{-1}$) for the relative group velocity $u_{\mathrm{g}}^*$ of symmetric disturbances. This value is significantly reduced for zonally confined disturbances ($\mathscr{F} = 0.25$ for $k = 2l$) and increased for zonally broad structures ($\mathscr{F} = 2.83$ for $k = l/2$).

The dispersion characteristics of surface edge waves prompt several *hypotheses* for (upstream) cyclone development:

(1) Larger-scale components ($k < l$) of a surface temperature anomaly have a relatively rapid eastward group velocity. Their vertical decay length ($1/\mu$) is comparatively large (typically 5 km) and they are more likely to interact with upper-level features. Hence a broad initial surface temperature disturbance leads to an eastward propagating large-scale primary cyclone which develops rapidly into a vertically deep system with considerable amplitude also at the tropopause level.

(2) Smaller-scale components ($k > l$) of a surface temperature anomaly have a small zonal group velocity and are vertically shallow. It is these components that are responsible for the genesis of the small and slowly traveling upstream cyclones just slightly to the east of the initial position of the initial perturbation. The associated intensification rate depends critically on the details of the initial perturbation (cf. Davies and Bishop, 1994).

(3) In the case of upper-level induced cyclogenesis (i.e., without an initial low-level perturbation) surface temperature anomalies are created during the evolution by the upper-level flow structures (as illustrated by simulation UL1 in Section 3). The surface wind field induced by narrow synoptic-scale upper-level troughs produces surface temperature anomalies with more intense small-scale components than the ones induced by broader planetary-scale troughs, and hence the former are more favorable for the genesis of upstream cyclones.

Note that these hypotheses are based upon a linear analysis of the properties of surface temperature perturbations within a uniform baroclinic zone. In the following, it is verified that these qualitative inferences hold for less idealized flow systems using a series of numerical experiments with different initial perturbations.

### *4.2. Surface induced sensitivity experiments*

In order to test hypotheses (1) and (2) simulations have been performed with surface temperature anomalies as initial perturbations. The surface flow evolution for simulations S1W and S2W (cf. Table 1) is shown in Fig. 5. In both cases the warm initial temperature anomaly has the same meridional scale, and for S1W (S2W) the zonal scale corresponds to twice (half) the meridional one. In order to initiate the simulations with an equally large temperature disturbance (integrated over the entire horizontal domain), the amplitude of the anomaly is four times larger in the case of S2W than for S1W. This leads to a more rapid evolution of S2W (see for instance Figs. 5b, f). A comparison of the two experiments relative to the evolution of the primary cyclone reveals strikingly different baroclinic wave developments and confirms the above mentioned hypotheses. Whereas in S1W two downstream (D1 and D2) and only a weak upstream depression appear until the occlusion of the mature primary system (Fig. 5c), only one downstream but two upstream features (U1 and U2) develop in the simulation S2W (Fig. 5f). The separation between the consecutive large-scale downstream cyclones in S1W corresponds to more than 6500 km compared to 2000 km for the small-scale upstream cyclones in S2W. Note that in S2W genesis of both upstream depressions occurs very close to the position of the initial disturbance, in agreement with the vanishing group velocity of edge waves in the limit of small zonal dimensions. On the other hand the structural evolution of the individual primary and secondary low-pressure systems and their attendant fronts is very similar to the upper-level induced experiment described in Section 3. Again the downstream developments have prominent upper-

* The meridional wavenumber has been chosen such that the wavelength corresponds to about twice the width of the baroclinic zone.

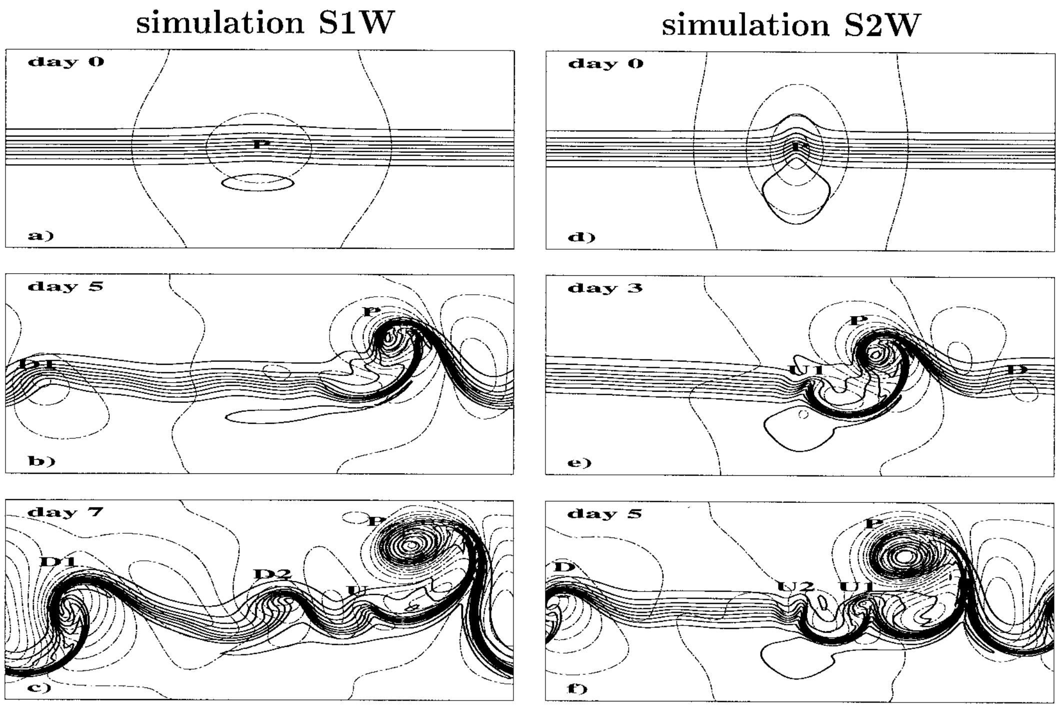


*Fig. 5.* Surface flow evolutions for the numerical simulations S1W (left panels) and S2W (right panels). Shown are the same fields as in the left panels of Fig. 2. Note that the middle and lower juxtaposed panels do not correspond to the same time instances, they have been chosen such as to illustrate a comparable phase of development of the primary cyclone.

level precursors whereas the upstream systems intensify initially below the unperturbed basic state jet (not shown).

A still more rapid development of a small-scale upstream cyclone can be obtained when the simulation is initiated with a narrow and *cold* surface temperature anomaly (simulation S2C). In this case the early development is dominated by the growth of an intense surface anticyclone, which leads to the genesis of a downstream cyclone U already at day 1.5, 12 h prior to the occurrence of a large-scale downstream system D (Fig. 6). This example underlines the importance of the anticyclonic flow induced by the cold surface anomaly for upstream cyclogenesis. (This mechanism of anticyclonic–cyclonic reversal has also been studied in isolation by Müller et al. (1989), who investigated the evolution of a localized cold anomaly in a baroclinically stable atmosphere.) Furthermore, simulation S2C indicates that the formation of an intense cold front associated with

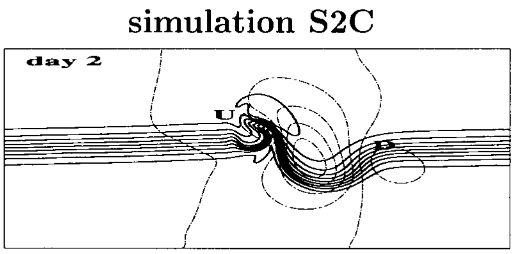


*Fig. 6.* Surface flow evolutions for the numerical simulations S2C at day 2. Shown are the same fields as in the left panels of Fig. 2.

a mature large-scale depression is not a prerequisite for the generation of upstream cyclones.

### 4.3. *Upper-level induced sensitivity experiments*

Two additional experiments of upper-level induced cyclogenesis are shown in Fig. 7 in order to assess the validity of hypothesis (3). Simulation

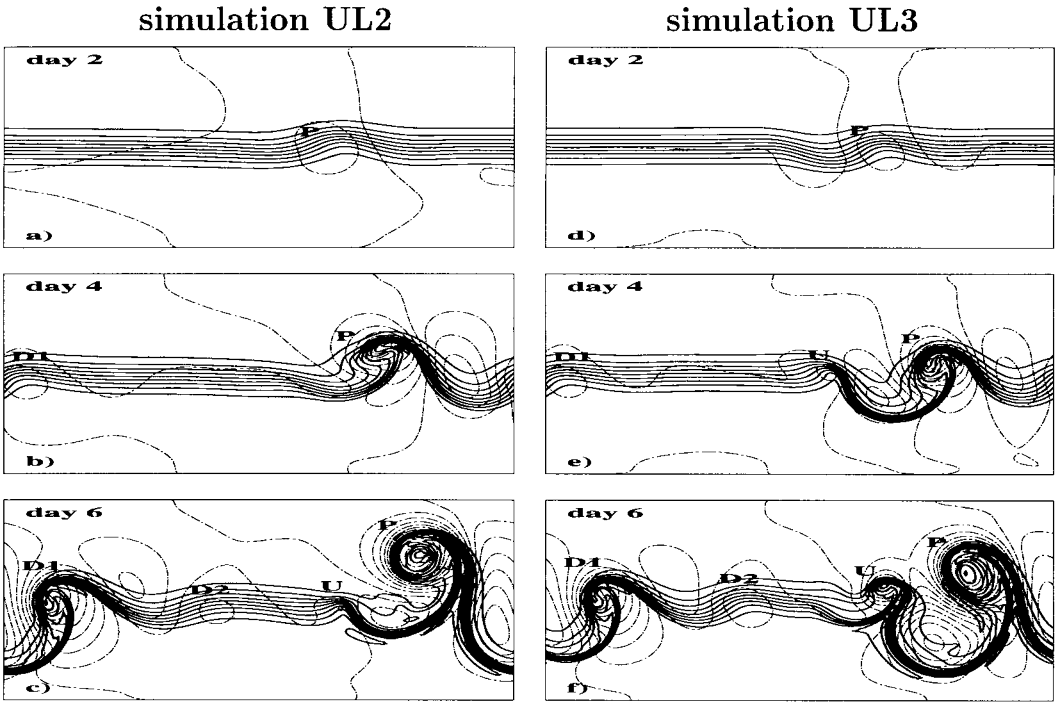


*Fig. 7.* Surface flow evolutions for the numerical simulations UL2 (left panels) and UL3 (right panels). Shown are the same fields as in the left panels of Fig. 2.

UL2 is initiated with a broader upper-level trough than UL1 (Table 1), and UL3 with a more narrow ridge-trough structure (a zonally aligned dipole of negative–positive PV anomalies). This setting has been chosen to induce a strong northerly flow at the surface and thereby to assist the rapid generation of a small-scale (cold) surface temperature anomaly. A comparison of the two simulations confirms hypothesis (3) and illustrates the stark effect of the scale of the upper-level initial perturbation on the evolution of upstream cyclones. As expected, in simulation UL3 a cold surface anomaly is generated early in the development to the west of the incipient primary cyclone (Fig. 7d), which leads to a prominent anticyclone at day 4 (Fig. 7e). At the same time an upstream cyclone U occurs in UL3, which develops into a mature small-scale secondary cyclone with a surface pressure minimum of 970 hPa by day 6 (Fig. 7f). This upstream development is significantly weaker in simulation UL2, where the upstream feature deepens only to 995 hPa by day 6 (Fig. 7c). Note on the other hand that the evolution of the primary (P) and the two downstream cyclones (D1, D2) and their attendant fronts is very similar in both simulations (the surface pressure values in the cyclone centers differ only by 1–2 hPa at day 6). This indicates that the genesis and evolution of small-scale upstream cyclones is particularly sensitive to the scale of the initial perturbation, whereas — at least within the investigated parameter range — upper-level induced synoptic-scale systems are almost unaffected.

## 5. Discussion

The influence of the scale of initial perturbations on the generation and development of upstream cyclones was studied within the framework of dry primitive equation dynamics. The results from a series of idealized channel model experiments confirm earlier findings on the characteristics of upstream cyclones and provide additional insight into the role of precursors for the genesis, evolution and structure of primary and secondary low pressure systems. The main conclusions are summarized and discussed in the next paragraphs, followed by a discussion of the shortcomings of the present methodology and of possible implications for related issues of extratropical cyclogenesis.

### *5.1. Characteristics of upstream (and downstream) development*

Numerical simulations over an extended time period within a long baroclinic channel show that an isolated upper-level perturbation (i.e., a positive PV anomaly) can not only directly induce a primary event of cyclogenesis (cf. the type-B classification of Petterssen and Smebye (1971) and the schematic by Hoskins et al. (1985, their Fig. 21)), but also indirectly a zonally-aligned train of high- and low-pressure systems that grow up- and downstream of the translating primary system. Within the PV framework this can be analyzed as dispersion of the initial tropopause-level PV anomaly (which leads to the "top-down" growing downstream systems) and of the induced surface temperature perturbations (leading to the "bottom-up" amplifying upstream cyclones).

The simulations corroborate several characteristics of up- and downstream cyclones that have been found in earlier studies (Simmons and Hoskins, 1979; Orlanski and Chang, 1993), for instance the sub-synoptic scale and more shallow structure of the upstream systems versus the upper-level induced, deep-reaching and large-scale downstream features. In addition it has been shown, for the present choice of a symmetric jet-like basic state, that downstream cyclones have a wide warm sector and pronounced T-bone surface frontal structure (cf. the terminology of Shapiro and Keyser (1990)) throughout the development, whereas the surface frontal evolution of upstream systems is characterized by intense warm fronts and a rapid occlusion process with cold fronts that form just before or during the occlusion process. Note that in this study distinct frontal and cyclone structures evolve from a localized initial perturbation within the same symmetric jet-like baroclinic zone, whereas the more traditional approach to study the variability of cyclone structures is to consider the sensitivity of only the primary baroclinic wave development upon the structure of the basic state (Hoskins and West, 1979; Davies et al., 1991; Thorncroft et al., 1993; Wernli et al., 1998) or upon different physical processes.

A more detailed investigation of the genesis and evolution of upstream cyclones based upon a linear analysis of surface edge waves and nonlinear numerical sensitivity experiments reveals the key role of small-scale* components in the surface temperature field which is either initially specified or induced during the early phase of the evolution by the initial upper-level perturbation. Whereas larger-scale components rapidly propagate to the east and interact with upper-level structures, smaller-scale components remain almost stationary (relative to the generally weak surface mean flow) and grow into shallow and subsynoptic-scale upstream cyclones. As a consequence initial conditions with a significant small-scale component are favorable for the occurrence of upstream cyclones whereas for instance broad upper-level troughs induce a baroclinic wave development without (or only with weak) upstream systems.

### *5.2. Caveats of the adopted approach*

However, the simplicity of the model and the approach adopted in this study place constraints upon the generality of the results. The simulations have been performed within a highly idealized setting and effects of the earth's sphericity as well as frictional and diabatic effects have been neglected. Several studies revealed the significant influence of physical processes on the structure and evolution of primary cyclones, and Orlanski and Chang (1993) have demonstrated that both surface friction and $\beta$ effects lead to a weakening of downstream development. Clearly the inclusion of surface friction for realistic oceanic conditions into the present type of experiments and complementary simulations on the sphere constitute important next steps to assess the robustness of the findings from the present study.

The simplest possible setting has been chosen in order to illustrate the sensitivity property of upstream development to the scale of the initial perturbation. This includes the choice of a zonally uniform and meridionally symmetric basic state

* As before the terms "small-" ("large-") scale are used for dimensions smaller (larger) than the width of the baroclinic zone.

jet, and the restriction to a particular shape of the initial perturbations. On the other hand it is known that the structure of the basic state plays a fundamental role for idealized baroclinic wave development (Davies et al., 1991; Thorncroft et al., 1993; Wernli et al., 1998; Shapiro et al., 1998), and it has been suggested that different archetypal cyclone life cycles can be related to the zonally nonuniform structure of the atmosphere (Schultz et al., 1998). The study by Schmidli (1997) revealed that upstream activity is enhanced (reduced) in the case of an additional anticyclonic (cyclonic) barotropic shear component in the basic state. This result is consistent with the present finding that the formation of strong surface anticyclones is favorable for upstream development. Further investigations are required to assess the relative importance of the basic state structure, the shape and scale of the nonmodal perturbations, and physical processes for the genesis and evolution of small-scale secondary systems.

### 5.3. *Further remarks*

As suggested by Simmons and Hoskins (1979) and discussed by Shapiro et al. (1998) upstream development can be considered as a theoretical interpretation of the Norwegian school paradigm of cyclone families (Bjerknes and Solberg, 1922). Fig. 5f has shown an example for the formation of a cyclone family (with two small-scale and shallow upstream systems) that evolved from an isolated initial perturbation. In the light of the shallow and "bottom-up" developing nature of upstream cyclones it is interesting to note that the Norwegian "frontal-wave concept of cyclogenesis did not accord with, nor account for, the observed upper-tropospheric signal of cyclones" (Davies, 1997). Furthermore, the mechanism of secondary frontal wave development proposed by Thorncroft and Hoskins (1990) has many similarities with the one proposed here. Note however that in the present simulations it is a *single* localized initial perturbation which initiates the simultaneous growth of large and small-scale cyclones and their attendant fronts, whereas the more classical theory of frontal wave instability (see for instance the review by Parker (1998)) has *2 distinct phases*: (1) large-scale primary systems grow through baroclinic instability processes and account for the formation of sharp fronts, and (2) these fronts are unstable and give birth to smaller secondary frontal-wave cyclones.

Upstream development is difficult to unambiguously identify in nature, due to the possible influences from physical processes in the lower atmosphere and from the variety of upper-level structures. Shapiro et al. (1998) analyzed the baroclinic wave development in the North Atlantic during 14–16 February 1997 and suggested that one of the secondary cyclones formed "through upstream development at the end of the trailing cold front of the primary synoptic-scale cyclone in the absence of an initial localized disturbance in the vicinity of the tropopause". Here we look briefly at two time instances of this FASTEX post IOP-15 period. At 00 UTC 16 February (Fig. 8b) the large-scale primary cyclone P is located to the

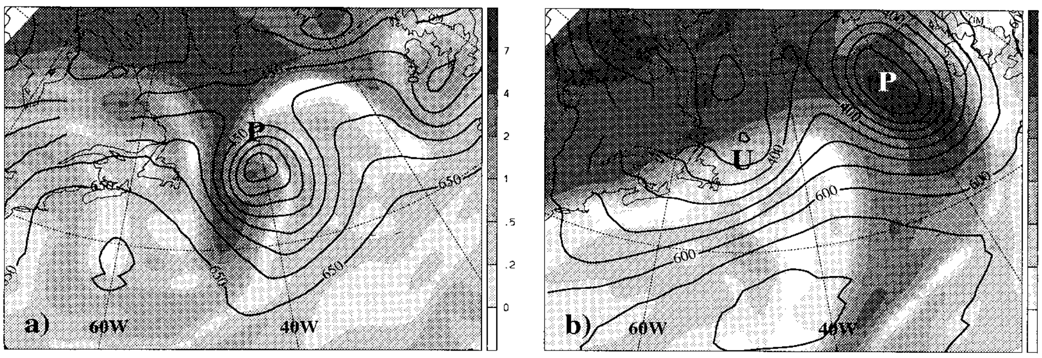


*Fig. 8.* ECMWF analysis fields valid at (a) 18 UTC 14 February and (b) 00 UTC 16 February 1997. Shown are upper-level PV (shaded, in pvu, see scale beside panels) and the geopotential height at 950 hPa (solid lines, contour interval 50 m). In (a) the upper-level PV is displayed on the 305 K isentropic surface and in (b) on 320 K.

west of Ireland below a prominent upper-level PV anomaly, and a weak secondary cyclone U can be observed to the east of Newfoundland near 50°W. Slightly to the west of this location a marked and narrow upper-level PV structure can be observed 30 h earlier (Fig. 8a). The zonally aligned dipole of zonally confined negative and positive PV anomalies corresponds qualitatively to the initial perturbation used in simulation UL3. This brief analysis supports the inference of Shapiro et al. (1998) that upstream development might be responsible for the formation of the secondary cyclone U. In addition, it indicates that the upper-level structures which are, as inferred from the this idealized study, favorable for upstream development can be of relevance in the real atmosphere.

The results of this paper also have some implications for the issue of the predictability of extratropical flow systems. The sensitivity of baroclinic wave development to the initial conditions seems to be highly selective, in that primary and downstream cyclones are almost unaffected by the scale of the imposed initial perturbation, whereas upstream depressions are particularly sensitive. It has been shown that the genesis and intensification of shallow small-scale cyclones can be crucially dependent upon the structure of an upper-level trough, via the induced surface temperature anomaly. By the time the upstream cyclone has reached a certain intensity, the initiating upper-level trough has moved to the east and is itself directly involved in a different event of cyclogenesis. This kind of dynamical relationship between shallow secondary cyclones and *downstream* features near the tropopause level has no counterpart among the various "conceptual models" currently utilized in synoptic meteorology and operational forecasting. In this context it is interesting to note that small-scale "secondary cyclones are often poorly forecast, and in extreme cases can have damaging consequences" (Parker, 1998).

## 6. Acknowledgments

We are grateful for the help of René Fehlmann to generate the initial conditions for the numerical experiments, and David N. Bresch for implementing the periodic version of the idealized model.

REFERENCES

Bishop, C. H. and Thorpe, A. J. 1994. Potential vorticity and the electrostatics analogy: quasi-geostrophic theory. *Quart. J. Roy. Meteor. Soc.* **120**, 713–731.

Bjerknes, J. and Solberg, H. 1922. Life cycles of cyclones and the polar front theory of atmospheric circulation. *Geofys. Publ.* **3**, 3–18.

Davies, H. C. 1976. A lateral boundary formulation for multi-level prediction models. *Quart. J. Roy. Meteor. Soc.* **102**, 405–418.

Davies, H. C. 1994. Theories of frontogenesis. In: *Proceedings of the International Symposium on the Life cycles of extratropical cyclones*, vol. I, pp. 182–192, Eds. S. Grønås and M. A. Shapiro, Bergen University, Bergen, Norway.

Davies, H. C. 1997. Emergence of the mainstream cyclogenesis theories. *Meteorol. Zeitschrift N. F.* **6**, 261–274.

Davies, H. C. and Bishop, C. H. 1994. Eady edge waves and rapid development. *J. Atmos. Sci.* **51**, 1930–1946.

Davies, H. C., Schär, C. and Wernli, H. 1991. The palette of fronts and cyclones within a baroclinic wave development. *J. Atmos. Sci.* **48**, 1666–1689.

Fehlmann, R. 1997. Dynamics of seminal PV elements. PhD thesis, Dissertation nr. 12229. ETH Zürich, Switzerland, 143 pp.

Hoskins, B. J. and West, N. V. 1979. Baroclinic waves and frontogenesis. Part II: Uniform potential vorticity jet flows. *J. Atmos. Sci.* **36**, 1663–1680.

Hoskins, B. J., McIntyre, M. E. and Robertson, A. W. 1985. On the use and significance of isentropic potential vorticity maps. *Quart. J. Roy. Meteor. Soc.* **111**, 877–946.

Majewski, D. 1991. The Europa-Modell of the Deutscher Wetterdienst. In: *Numerical methods in atmospheric models*, vol. II, pp. 167–191. ECMWF, Reading UK.

Müller, J. C., Davies, H. C. and Schär, C. 1989. An unsung mechanism for frontogenesis and cyclogenesis. *J. Atmos. Sci.* **46**, 3664–3672.

Orlanski, I. and Chang, E. K. M. 1993. Ageostrophic geopotential fluxes in downstream and upstream development of baroclinic waves. *J. Atmos. Sci.* **50**, 212–225.

Parker, D. J. 1998. Secondary frontal waves in the North Atlantic region. A dynamical perspective of current ideas. *Quart. J. Roy. Meteor. Soc.* **124**, 829–856.

Petterssen, S. and Smebye, S. J. 1971. On the development of extratropical cyclones. *Quart. J. Roy. Meteor. Soc.* **97**, 457–482.

Schmidli, J. 1997. *The effect of barotropic shear on cyclones, fronts and tropopause structures — numerical simulations with a primitive equation model.* Diploma thesis. Atmospheric Physics ETH, Zürich, Switzerland, 85 pp.

Schultz, D. M., Keyser, D. and Bosart, L. F. 1998. The effect of large-scale flow on low-level frontal structure and evolution in midlatitude cyclones. *Mon. Wea. Rev.* **126**, 1767–1791.

Shapiro, M. A. and Keyser, D. 1990. Fronts, jet streams and the tropopause. In: *Extratropical cyclones. The Erik Palmen Memorial Volume*, pp. 167–191, Eds. C. Newton and E. O. Holopainen. Amer. Met. Soc., Boston, USA.

Shapiro, M. A., Wernli, H., Bao, J.-W., Methven, J., Zou, X., Neiman, P. J., Donall-Grell, E., Doyle, J. D. and Holt, T. 1998. A planetary-scale to mesoscale perspective of the life cycles of extratropical cyclones: The bridge between theory and observations. In: *The life cycles of extratropical cyclones*, pp. 139–185, Eds. S. Grønås and M. A. Shapiro. Amer. Met. Soc., Boston, USA.

Simmons, A. J. 1994. Numerical simulations of cyclone life cycles. In: *Proceedings of an International Symposium on the Life cycles of extratropical cyclones*, vol. I, pp. 149–160, Eds. S. Grønås and M. A. Shapiro, Bergen University, Bergen, Norway.

Simmons, A. J. and Hoskins, B. J. 1979. The downstream and upstream development of unstable baroclinic waves. *J. Atmos. Sci.* **36**, 1239–1254.

Thorncroft, C. D. and Hoskins, B. J. 1990. Frontal cyclogenesis *J. Atmos. Sci.* **47**, 2317–2336.

Thorncroft, C. D., Hoskins, B. J. and McIntyre, M. E. 1993. Two paradigms of baroclinic-wave life-cycle behaviour. *Quart. J. Roy. Meteor. Soc.* **119**, 17–56.

Wernli, H., Fehlmann, R. and Lüthi, D. 1998. The effect of barotropic shear on upper-level induced cyclogenesis: semigeostrophic and primitive equation numerical simulations. *J. Atmos. Sci.* **55**, 2080–2094.